

Interpolation of unitaries with time-dependent Hamiltonians via Deep Learning

Antonio Guerra¹, Daniel Uzcategui-Contreras², Aldo Delgado¹,
Esteban S. Gómez¹

¹Departamento de Física e Instituto Milenio de Investigación en Óptica, Universidad de Concepción, Casilla 160-C, Concepción, Chile

²Departamento de Matemática y Física Aplicadas, Universidad Católica de la Santísima Concepción, Alonso de Ribera 2850, Concepción, Chile

Abstract

Quantum systems governed by time-dependent Hamiltonians pose significant challenges for the accurate computation of unitary time-evolution operators, which are essential for predicting quantum state dynamics. In this work, we introduce a physics-informed deep learning approach based on Physics-Informed Neural Networks to estimate these operators over the full time domain. By incorporating physical constraints such as unitarity and leveraging the second-order Magnus expansion on the evolution operator, the proposed framework enables the estimation of unitary matrices at different time intervals. The model is trained using simulated unitary operators and evaluated on quantum systems ranging from 2 to 6 qubits. For larger many-body systems, specifically those with 7 and 8 qubits, the same methodology is employed to reconstruct an effective time-dependent Hamiltonian, from which the corresponding time-evolution operator is computed over the entire temporal domain. The proposed framework achieves fidelities exceeding 0.92 using a limited number of unitary samples, indicating a potential reduction in measurement and data acquisition costs. These results highlight the effectiveness of the approach for data-driven simulation and identification of quantum dynamical systems, with direct relevance to quantum computing and quantum simulation applications.

1 Introduction

Over the past decade, advances in Artificial Neural Networks (ANNs) and Deep Learning (DL) have enabled solutions to computational problems previously considered intractable [1, 2]. These methods now have wide application across the physical sciences, including materials discovery [3], climate modeling [4], and medical diagnostics [5, 6]. Within physics, neural networks have been successfully applied to the analysis of high-dimensional collider data [7], gravitational wave detection [8], quantum state reconstruction from measurements [9, 10], the combination of marginals into global quantum states [11], and the solution of differential equations through Physics-Informed Neural Networks (PINNs) [12]. These developments illustrate the growing versatility of machine learning models for modeling and simulating complex physical systems.

A fundamental challenge in quantum physics is the accurate modeling of the dynamics of high-dimensional quantum systems, particularly many-body systems, under time-dependent interactions described by time-dependent Hamiltonians $H(t)$. Such Hamiltonians play a central role in quantum technologies, including quantum control and gate optimization [13], as well as quantum simulations of complex many-body systems [14]. The simulation of time-dependent quantum dynamics is hindered by several factors: the non-commutativity of Hamiltonians at different times requires explicit time ordering, analytic solutions typically rely on infinite series expansions, numerical methods exhibit unfavorable scaling with system size, and numerical errors tend to accumulate over long evolution times.

Several approaches have been developed to address quantum evolution driven by time-dependent Hamiltonians. Methods based on truncated Taylor and Dyson series expansions of the evolution operator have shown promising results [15, 16]. Modified Suzuki–Trotter decompositions have been proposed for interpolating unitary operators in time-dependent settings [17]. In quantum control, Magnus-expansion-based techniques have proven

particularly effective [18]. More recently, machine learning approaches, including PINNs, have been explored to learn quantum dynamics under physical constraints [19], as well as to reconstruct time-dependent Hamiltonians using deep learning models [20, 21].

Here, we introduce a complementary and flexible deep-learning-based approach to model the dynamics of quantum systems driven by time-dependent Hamiltonians. Our method is based on the Physics-Informed Neural Network (PINN) framework, in which known physical constraints are explicitly incorporated into the training process to guide the learning of physically consistent solutions. We develop and evaluate models for systems ranging from 2 to 8 qubits. For systems with up to 6 qubits, the model directly learns the unitary time-evolution operator. For larger systems with 7 and 8 qubits, where the number of parameters becomes prohibitively large, the model is instead trained to predict an effective time-dependent Hamiltonian, from which the corresponding unitary operator is computed using either the Magnus expansion or Trotterization. This hybrid strategy allows the approach to scale to larger system sizes while maintaining a manageable computational cost.

A notable feature of the proposed framework is its ability to achieve high fidelity across the entire time domain, even when trained on datasets containing a small number of temporal samples. Models trained with coarse temporal discretizations (e.g., $\Delta t = 1.0$) exhibit fidelities comparable to those trained with finer discretizations (e.g., $\Delta t = 0.1$), demonstrating strong interpolation capabilities. These results indicate that, unlike conventional numerical solvers, the proposed deep-learning-based framework can reconstruct the full time-evolution operator from limited information while significantly reducing computational overhead. When tested on randomly generated time-dependent Hamiltonians, the models consistently exhibit high average fidelity with minimal variability.

This article is organized as follows. In Section 2, we present the theoretical background. Section 3 introduces the deep learning models used in this work, including their architectures, training procedures, and performance metrics. In Section 3.4, we analyze the accuracy of the proposed approach for different system sizes. Section 4 summarizes our conclusions and outlines potential future research directions. Finally, A provides a detailed description of the model architecture. All source code used in this work is publicly available on GitHub [22].

2 Quantum dynamics with time-dependent Hamiltonians

The state of a quantum system is described by a density operator ρ which is a normalized ($\text{Tr}(\rho) = 1$) positive semi-definite ($\rho \geq 0$) linear operator. This operator provides a complete description of a quantum system. An isolated quantum system, when subjected to an interaction described by a time-dependent Hamiltonian $H(t)$, evolves according to the von Neumann equation

$$\frac{d}{dt} \rho(t) = -\frac{i}{\hbar} [H(t), \rho(t)], \quad (1)$$

where \hbar is the reduced Planck constant. The general solution of Eq. 1 is given by

$$\rho(t) = U(t, t_0) \rho(t_0) U^\dagger(t, t_0), \quad (2)$$

with $U(t, t_0)$ the unitary evolution operator defined as

$$U(t, t_0) = \mathcal{T} \exp \left(-\frac{i}{\hbar} \int_{t_0}^t H(\xi), d\xi \right), \quad (3)$$

where the time-ordering operator \mathcal{T} ensures the proper ordering of Hamiltonian terms when the Hamiltonian at different times does not commute; that is, if $[H(t), H(t')] \neq 0$ for any $t \neq t'$. For the sake of simplicity, we assume $t_0 = 0$, such that $U(t, t_0) = U(t)$.

The evolution operator given by Eq. (3) can be written in different forms, such as using the Dyson series, the Magnus expansion, or the Trotter decomposition, among others. In this work, we focus on the Magnus expansion, which is particularly useful for time-dependent Hamiltonians, and on the Trotter decomposition, which is widely used in quantum computing and quantum simulation.

Therefore, in the Magnus approach, the evolution operator can be written as

$$U(t) = \exp \left(\sum_{i=1} \mathcal{O}_i(t) \right), \quad (4)$$

where, up to second order, the elements $\mathcal{O}_i(t)$ are given by

$$\mathcal{O}_1(t) = -\frac{i}{\hbar} \int_{t_0}^t H(\tau_1) d\tau_1, \quad (5)$$

$$\mathcal{O}_2(t) = \frac{1}{2} \left\{ -\frac{i}{\hbar} \right\}^2 \int_{t_0}^t d\tau_1 \int_{t_0}^{\tau_1} d\tau_2 [H(\tau_1), H(\tau_2)]. \quad (6)$$

Alternatively, the Trotterization approach discretizes the time interval, which leads to approximate the evolution operator as

$$U(t) \approx \overleftarrow{\prod}_{m=0}^{n-1} \left(\exp \left(-\frac{i}{\hbar} H(t_m) \Delta t \right) \right), \quad (7)$$

where $t_m = m\Delta t$, $\Delta t = t/n$, and n is the number of time steps in the discretization. The arrow on the product indicates that the product is ordered from right to left, with the smallest index on the right.

2.1 N-qubit systems

Operators acting on a N -qubit Hilbert space can be spanned using the N -fold tensor product of the Pauli basis $B = \{I, \sigma_x, \sigma_y, \sigma_z\}$. Thus, any Hamiltonian $H(t)$ acting in this space can be expressed as a linear combination of the basis elements of the N -fold tensor product $B^{\otimes N}$, that is,

$$H(t) = \hbar \sum_{\vec{\alpha} \in B} c_{\vec{\alpha}}(t) \sigma_{\vec{\alpha}}, \quad (8)$$

where $c_{\vec{\alpha}}(t)$ are coefficients with real value, and $\sigma_{\vec{\alpha}} = \sigma_{\alpha_1} \otimes \cdots \otimes \sigma_{\alpha_N}$ denotes the tensor product of Pauli matrices acting on each qubit. Since Eq. (1) describes the evolution of the density matrix as a differential equation, introducing explicit time dependence into the Hamiltonian may introduce additional complexities, such as nonlinear dynamics or externally induced oscillations, as observed, for instance, in nuclear magnetic resonance. In such situations, Floquet theory provides a rigorous framework for analyzing periodically driven quantum systems by studying their effective dynamics under a time-periodic Hamiltonian [23, 24].

We consider two types of Hamiltonians across different many-body configurations. For systems with up to six qubits, we employ a general Hamiltonian that includes all possible Pauli components in the expansion given by Eq. (8). For systems with seven or eight qubits, we restrict the Hamiltonian to an Ising model with nearest-neighbor interactions. The time-dependent coefficients are defined as

$$c_{\vec{\alpha}}(t) = A_{\vec{\alpha}} \sin(\omega_{\vec{\alpha}} t + \phi_{\vec{\alpha}}), \quad (9)$$

where $A_{\vec{\alpha}}$, $\omega_{\vec{\alpha}}$, and $\phi_{\vec{\alpha}}$ are randomly sampled parameters [22]. Naturally, once the parameters of a given Hamiltonian are selected, they are kept fixed throughout the entire design and training of the model. However, when considering different physical systems or exploring alternative dynamical regimes, the use of randomly sampled coefficients allows us to generate a diverse ensemble of time-dependent Hamiltonians. This strategy prevents the model from overfitting to specific dynamical patterns and ensures that the learned dynamics are not biased toward particular system realizations. As a result, the proposed approach enables a systematic assessment of the model's ability to generalize across a broad class of physically valid quantum systems, rather than being tailored to a single fixed Hamiltonian.

3 Model description

The rationale for employing PINNs lies in their capability to incorporate physical and mathematical constraints directly into the training process. PINNs have demonstrated outstanding performance in solving nonlinear differential equations and in modeling complex dynamical systems [12, 25]. Furthermore, neural networks consistently exhibit advantages in interpolation accuracy and adaptability to complex boundary and initial condition constraints.

We employ a model that generates a unitary complex-valued matrix from a scalar input. The dimensionality of these matrices increases exponentially with the number of qubits as 4^N . Figure 1 shows the number of trainable

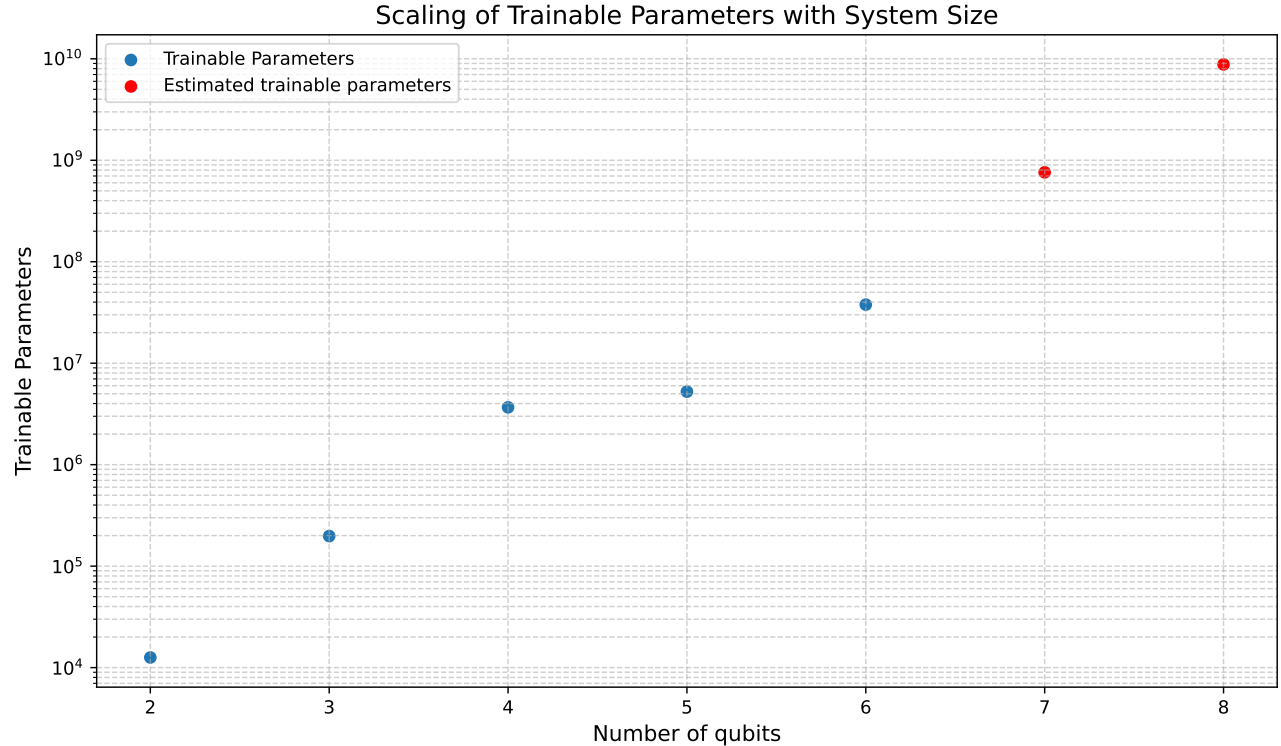


Figure 1: Amount of trainable parameters as a function of the number N of qubits. In cases with up to 6 qubits, this relationship is outlined. For systems containing 7 and 8 qubits, we have provided the estimated number of trainable parameters required to apply the same strategy to determine the unitary evolution operator for those systems.

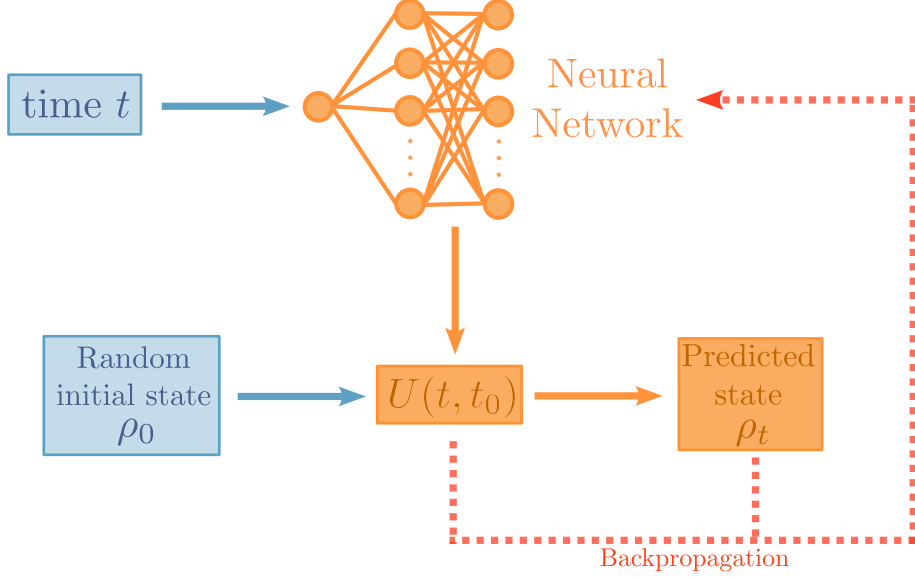
parameters for models up to 6-qubits, as well as the estimated parameter counts required for 7- and 8-qubit systems. Since the optimization process becomes computationally intractable at larger scales, an alternative strategy is adopted for these higher-dimensional cases. Rather than merely constraining the Hamiltonian to a reduced set of components, the model is constructed to estimate an effective time-dependent set of coefficients defining the effective Hamiltonian of the system $H_{\text{eff}}(t)$. Subsequently, with a model capable of generating $H_{\text{eff}}(t)$, we can use it to compute the time-evolution operator through (i) the Magnus expansion or (ii) the Trotter decomposition. This approach reduces the number of trainable parameters to approximately 10^3 .

3.1 Architecture description

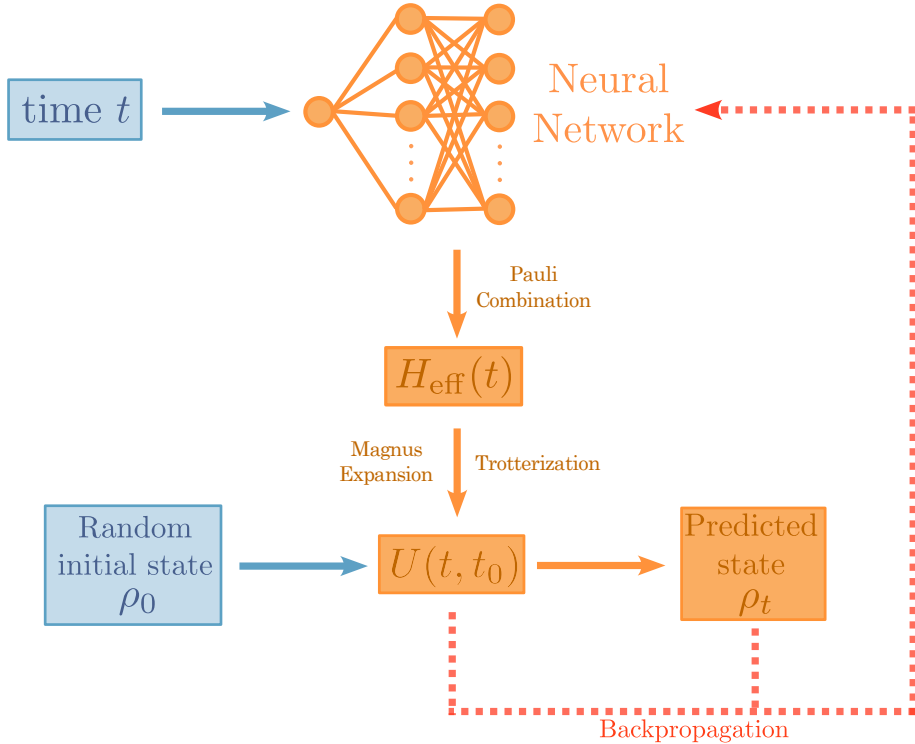
For the model architecture, we employ a straightforward approach consisting of a sequence of fully connected layers designed to match the number of parameters required for the output matrix. The hyperbolic tangent function is used as the activation function. This architecture can generate arbitrarily complex-valued matrices, ensuring that the model can accurately represent any matrix form of the time-evolution operator. Figure 2 schematically illustrates the two modeling strategies adopted for the time-evolution operator. A detailed description of the architectures used in the different models is provided in A.

3.2 Loss function and data generation

To train the model, a valid dataset is required. The dataset generation process is inspired by the idea that it can be interpreted as the outcome of multiple quantum process tomography (QPT) experiments performed at different times [26]. If the goal is to perform a quantum control task, the dataset will consist of a set of quantum states forming a trajectory and target unitary operators applied at specific times t . However, for practical purposes, the dataset is generated numerically by computing the system dynamics using Eqs. (2) and (3).



(a) PINN model for 2 to 6 qubits.



(b) PINN model for 7 and 8 qubits.

Figure 2: Illustration of two different methods for simulating the dynamics of quantum systems. (a) The method using PINN is applied to systems up to six qubits, where the model's role is to directly predict the unitary $U(t, t_0)$. (b) For instances involving seven or eight qubits, a different strategy is adopted, in which the model estimates the Pauli components of the effective Hamiltonian $H_{\text{eff}}(t)$, which changes over time, aiding the numerical determination of $U(t, t_0)$. The light blue shade indicates values prior to the model's application, the orange shade signifies the model and the outcomes post-calculation using the model's results, while the red shade denotes backpropagation, which involves comparing the procedure's outcomes with known theoretical values.

Employing the Magnus expansion or the Trotterization method increases the computational cost, as these calculations must be performed at each training iteration to update the model parameters. To mitigate this, the Magnus expansion is truncated at second order. For both the Magnus and Trotter approaches, we use 50 integration steps per model query, i.e., each time the model produces an output.

Furthermore, a single QPT is insufficient to accurately characterize $U(t)$. In principle, achieving near-perfect fidelities over a continuous time domain would require an infinite number of QPTs due to its continuous nature. Nevertheless, models such as the one proposed here help to significantly reduce the required measurement cost. The study focuses on the time interval $t \in [0, 1]$, employing discrete time grids with step sizes of $\Delta t = 0.1, 0.25, 0.5$, and 1.0. This procedure yields a comprehensive dataset for the selected time values, essential for effective model training. A training dataset $\{(\rho_0^i, \tau_i, \rho_{\tau_i}^i, U_{\tau_i})\}_{i=1}^{N_S}$, with $N_S = 11,000$ was generated, where the target unitaries U_{τ_i} are known and the evolved states satisfy $\rho_{\tau_i}^i = U(\tau_i, 0) \rho_0^i U^\dagger(\tau_i, 0)$. The evolution times $\tau_i \in [0, 1]$ are sampled from uniform time grids corresponding to different choices of the time step Δt .

The loss function is defined as an objective function whose minimization yields the optimal parameters of the deep learning model, such that the resulting model accurately describes the dynamics of the physical system under consideration. It is constructed to explicitly incorporate the known physical constraints governing the system dynamics, as well as the available supervision data. In particular, it enforces consistency with unitary quantum evolution, agreement with known unitary operators when available, and compliance with the von Neumann equation (1). The total loss function is defined as

$$\begin{aligned} \mathcal{L} = & \frac{1}{N_S} \sum_{i=1}^{N_S} \left(\left\| \rho_{\tau_i}^i - U_\theta(\tau_i) \rho_0^i U_\theta^\dagger(\tau_i) \right\| + \|U_\theta(\tau_i) - U_{\tau_i}\| \right) \\ & + \frac{1}{N_f} \sum_{k=1}^{N_f} \left\| \mathbb{1} - U_\theta(t_k) U_\theta^\dagger(t_k) \right\|, \end{aligned} \quad (10)$$

where $\|A\| = \sum_{ij} |a_{ij}|$ denotes the element-wise ℓ_1 matrix norm for any matrix $A = [a_{ij}]$, and $U_\theta(t)$ represents a neural network parametrization of the time-evolution operator with trainable weights $\theta = \{\theta_i\}$. Physics-Informed Neural Networks employ such neural representations to approximate unknown physical quantities while enforcing governing equations and constraints directly through the loss function [12].

Here, N_S denotes the number of available state-unitary training pairs, while N_f corresponds to the number of temporal collocation points used to enforce unitarity across the time domain. The first term of the loss enforces accurate quantum state evolution under the predicted unitary operator U_θ . The second term promotes consistency between the predicted unitaries and known target unitaries, when such information is available. The third term explicitly imposes the physical constraint of unitarity by penalizing deviations from $U_\theta(t) U_\theta^\dagger(t) = \mathbb{1}$ at arbitrary times.

For the 7- and 8-qubit systems, only the first two terms are employed. This choice is motivated by the fact that both the Magnus expansion and the Trotter decomposition intrinsically preserve unitarity, rendering an explicit unitarity penalty unnecessary in these cases. Although all results presented in this work are obtained using the full loss function in Eq. (10), we observe that satisfactory model performance can be achieved using only a subset of these terms. In this study, we focus on the most favorable training scenario, in which both the target unitary operators and the corresponding evolved quantum states are available during training.

3.3 Test and training

The AdamW optimizer is used for training, initialized with a learning rate of 10^{-3} . To enhance convergence stability, a learning-rate scheduler decreases the rate by a factor of 10^{-1} every 300 epochs. The training process spans 10^3 epochs, each consisting of 100 data batches with a batch size of 10. Each data set contains 11000 uniformly distributed tuples in the specified time intervals. In addition, the data batches used to train the models for seven- and eight-qubit systems are reduced to 10 data batches per epoch.

All models presented in this work were trained using an NVIDIA Quadro P6000 GPU. Figures 3 and 4 illustrate the evolution of the loss function over training epochs for different model sizes and datasets. It is important to note that for all model sizes, when the dataset is characterized by a larger Δt , the decrease in the loss function is more pronounced. This outcome is expected because the dataset is less constrained, leading to multiple tuples with fewer distinct times. However, our goal is to develop a model that can accurately interpolate between known times to predict unknown unitary matrices. Therefore, a more constrained model, with a smaller Δt , tends to yield better interpolation accuracy.

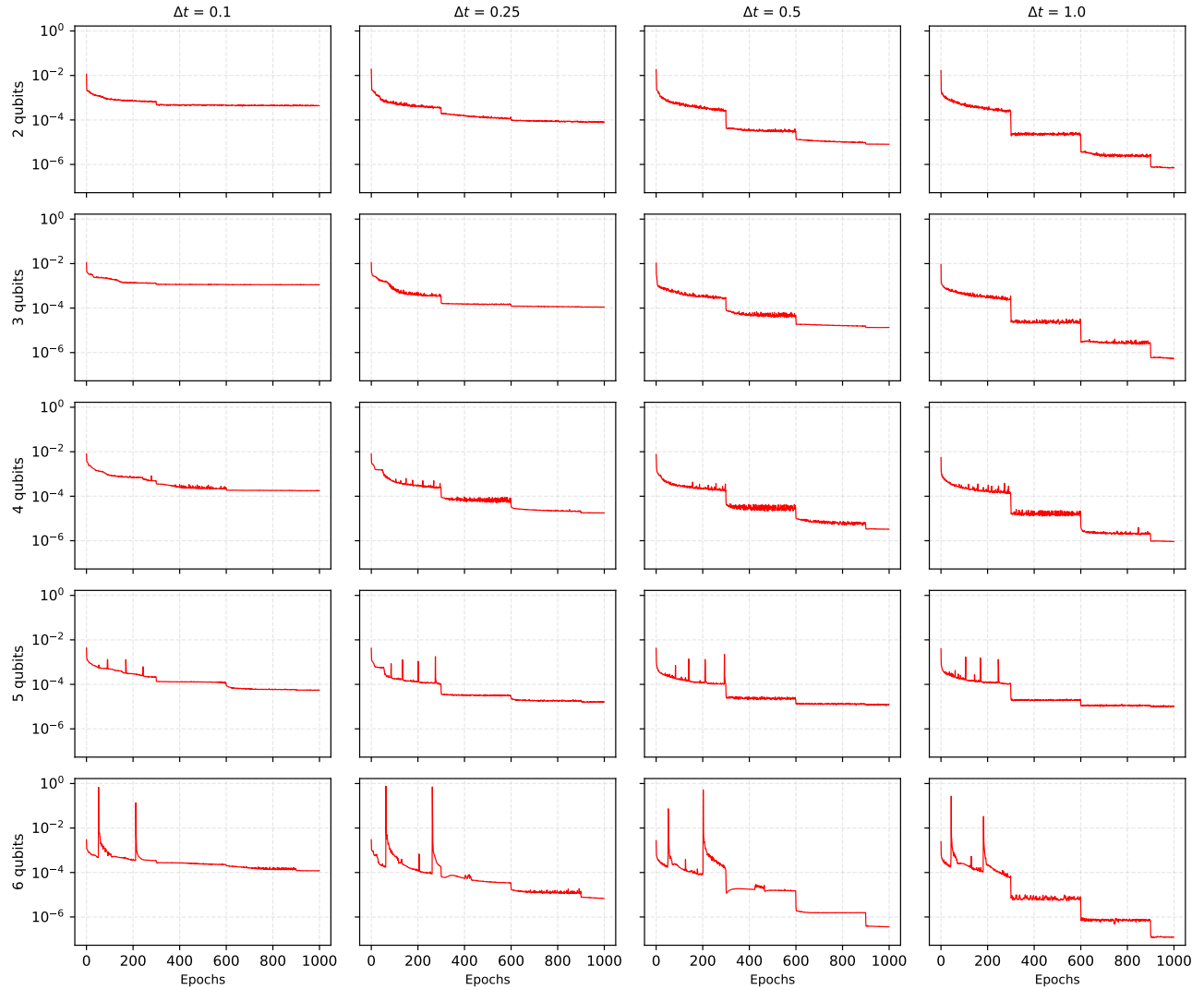


Figure 3: Curves of the loss function are depicted for configurations of 2-qubit to 6-qubit sizes, as well as for each of the four different training setups.

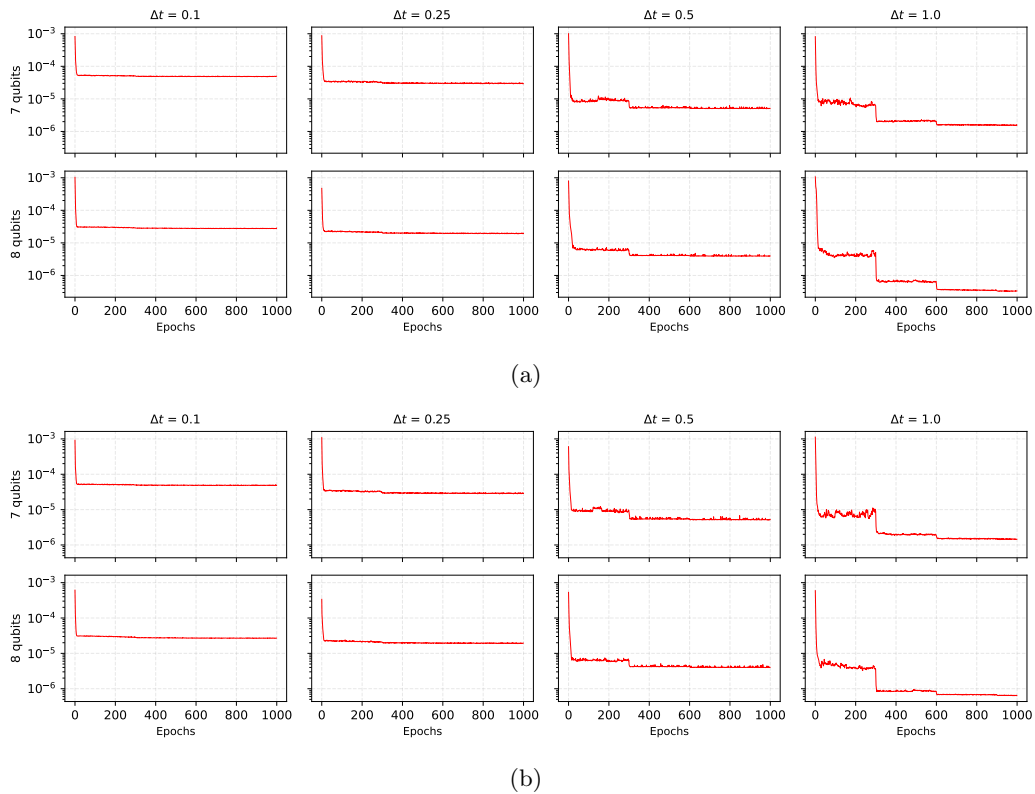


Figure 4: Loss function curves for 7- and 8-qubit configurations under the four training setups considered. Panel (a): Trotterization. Panel (b): Magnus expansion.

3.4 Results

To assess the model's performance over the entire time domain, we compute 100 target unitary matrices using the second-order Magnus expansion. These matrices are uniformly spaced in time and include values not present in the training set, thereby allowing us to rigorously evaluate the model's interpolation capability. To quantify accuracy, we adopt the gate fidelity [27], defined as

$$F(U(t), U_{\theta_{\text{opt}}}(t)) = \left| \frac{1}{d} \text{Tr} [U^\dagger(t) U_{\theta_{\text{opt}}}(t)] \right|^2, \quad (11)$$

where θ_{opt} are the optimal weights of the Neural Network found during training, and $d = 2^N$ denotes the Hilbert-space dimension for an N -qubit system. The fidelity ranges from 0 to 1, with $F = 1$ only when the predicted operator $U_{\theta_{\text{opt}}}(t)$ coincides with the target $U(t)$ at time t .

For evaluation, each trained model generates unitary matrices at the same 100 time points. These predicted matrices are then compared one-by-one with the target unitaries, yielding a fidelity function $F(t)$. Since multiple models for each system size are trained with different values of Δt , four fidelity curves $F(t)$ are obtained for each system size.

The loss function additionally enforces unitarity across the time domain, ensuring that the model's predictions remain close to unitary transformations throughout training. To further minimize numerical deviations, we can compute the closest unitary matrix to each predicted output via Singular Value Decomposition (SVD), redefining the estimated unitary as

$$U_{\theta_{\text{opt}}}(t) = U V_h, \quad (12)$$

where U and V_h arise from the SVD of the model's predicted matrix. The following results compare the performance of the different models with and without post-processing, showing that high fidelity is preserved even in the absence of the closest-unitary correction.

The results in Fig. 5 summarize the fidelity performance for systems up to 6-qubits with and without the error correction via (12). As expected, datasets with smaller time steps (Δt) achieve the highest fidelities due to their finer temporal resolution. Nevertheless, even for larger Δt , the reduction in fidelity remains minimal. This reflects the PINN's strong interpolation capability, which maintains an accurate approximation of the quantum dynamics even with coarse temporal discretization.

For the 7- and 8-qubit cases, the model follows a different strategy by estimating an effective Hamiltonian as an intermediate step to compute the corresponding unitary matrix. Since the evolution can be obtained either through Trotterization or the Magnus expansion, both approaches were implemented and evaluated independently. Also, since Trotterization and Magnus expansion ensure unitarity of the model's output, it's not necessary to include SVD post-processing error correction. Figure 6 shows the fidelity results for these higher-dimensional systems across different training datasets. Consistent with the behavior observed in Fig. 5, even for large values of Δt , the degradation in fidelity is minimal, demonstrating that the interpolation remains highly effective in all tested scenarios.

To ensure that our evaluation did not rely on a single Hamiltonian realization per system size, we performed an additional statistical analysis to assess the model's robustness in interpolating unitary dynamics across diverse configurations. For system sizes up to 6-qubits, we carried out 100 independent training runs. Due to computational resource constraints, this analysis was limited to 50 independent runs for 7- and 8-qubit systems. In each run, the amplitudes, frequencies, and phases defining the Hamiltonian were randomly sampled. This corresponds to $4^N - 1$ independent parameters for systems of up to 6-qubits, and to $2N - 1$ parameters for the 7- and 8-qubit Ising Hamiltonians. These parameters were used to construct the target unitary evolutions, generate the corresponding training datasets, and train the model under identical conditions. Applying the same fidelity-evaluation pipeline yielded a collection of fidelity curves $F^{(k)}(t)$ for each system size. The mean fidelity $F_\mu(t)$ and the fidelity standard deviation $F_\sigma(t)$ were computed as

$$F_\mu(t) = \frac{1}{N} \sum_{k=1}^N F^{(k)}(t), \quad (13)$$

$$F_\sigma(t) = \sqrt{\frac{1}{N-1} \sum_{k=1}^N \left(F^{(k)}(t) - F_\mu^{(k)}(t) \right)^2}, \quad (14)$$

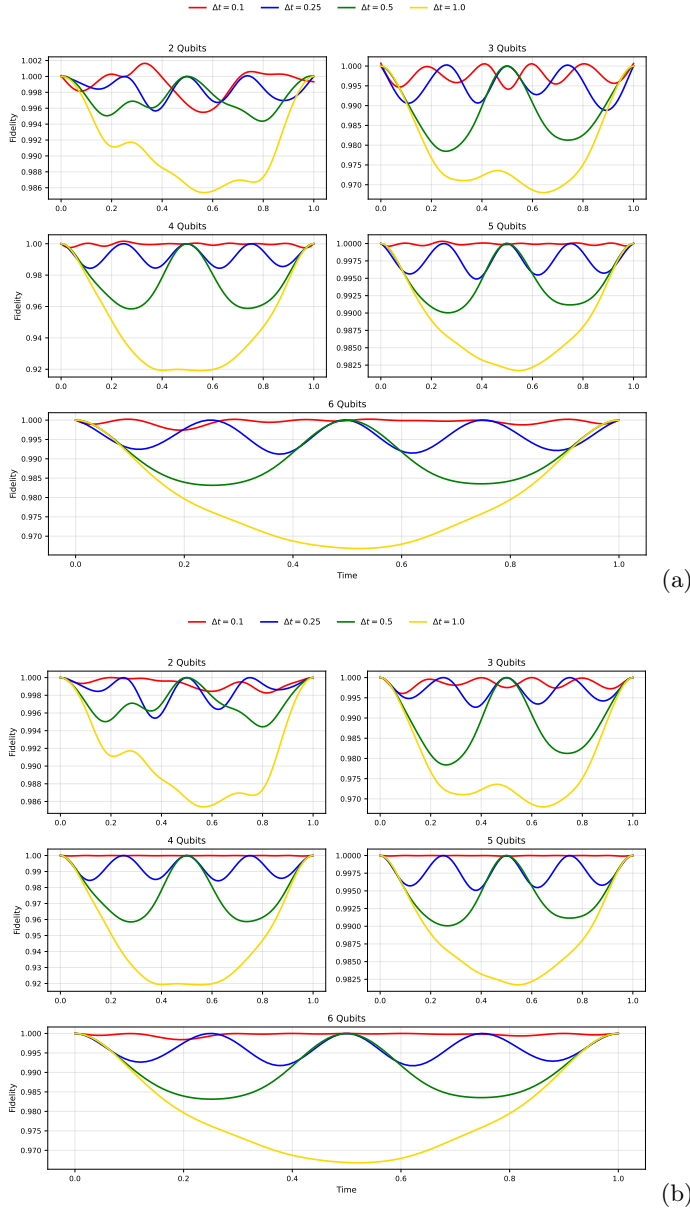


Figure 5: Fidelity of the predicted unitary evolution for model2–model6, shown (a) before and (b) after SVD-based post-processing error correction.

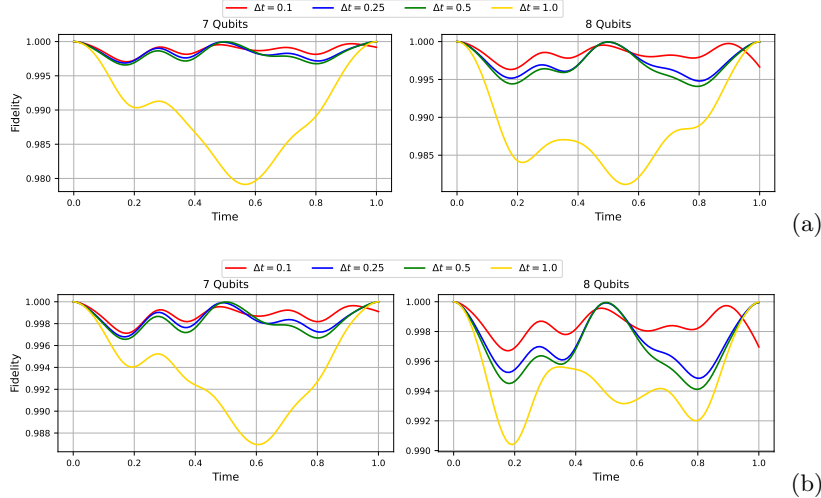


Figure 6: Fidelity performance for 7- and 8-qubit systems under the four training setups considered. (a) Trotter-based model. (b) Magnus-based model.

where $U^{(k)}(t)$ denotes the target unitary computed at time t via Eq. (7), and $U_{\theta_{\text{opt}}}^{(k)}(t)$ is the unitary predicted by the model at time t .

Figure 7 summarizes the mean fidelity and standard deviation across all independent runs, providing a quantitative assessment of the variability in the model’s performance. For each system size, two panels are shown: the first compares the raw model outputs with the target unitary evolutions, while the second reports the nearest-unitary matrices obtained through SVD-based post-processing. For the 7- and 8-qubit systems, the inclusion of SVD error correction does not lead to a noticeable performance improvement. This behavior is expected, since the target evolutions are generated using Trotterization and Magnus-based constructions, which enforce unitarity by design.

Since these results closely match those obtained in the single-training analysis, we expect a similar statistical behavior for other values of Δt when applying the same procedure. Additionally, for the 7- and 8-qubit cases, Trotterization was employed instead of the Magnus expansion for computational efficiency.

Across all analyses, the standard deviation remains consistently low. Even without enforcing unitarity via SVD, the variability is small, and after error correction the associated uncertainty becomes negligible—particularly for systems up to 6 qubits, where it is not visually distinguishable in the figure. Moreover, no specific regions were identified where the model failed to interpolate successfully. These results indicate that, given sufficient training data, the model is able to robustly learn the underlying quantum dynamics.

4 Conclusions and remarks

In this work, we introduced a fully connected framework designed to learn and emulate the temporal evolution of many-body quantum systems governed by time-dependent Hamiltonians. By employing Physics-Informed Neural Networks (PINNs), the model incorporates physical constraints directly into the loss function, enabling it to capture the underlying quantum dynamics. The proposed architecture takes a single scalar input and outputs $2^{(N+1)}$ parameters corresponding to the unitary evolution operator. Due to the exponential scaling of the network size with the number of qubits, models were explicitly trained up to 6 qubits. For the 7- and 8-qubit cases, the Hamiltonian was simplified to include only X and Z components, allowing the unitary evolution to be efficiently computed using either a second-order Magnus expansion or a Trotter decomposition. This reduction significantly lowers the number of trainable parameters and renders the problem computationally tractable. The results presented in Section 3.4 demonstrate that PINNs are capable of accurately interpolating the quantum dynamics encoded in the training data.

To reduce the measurement cost associated with data generation, we adopted a strategy based on quantum process tomography (QPT) performed at uniformly spaced time intervals. This approach is substantially more

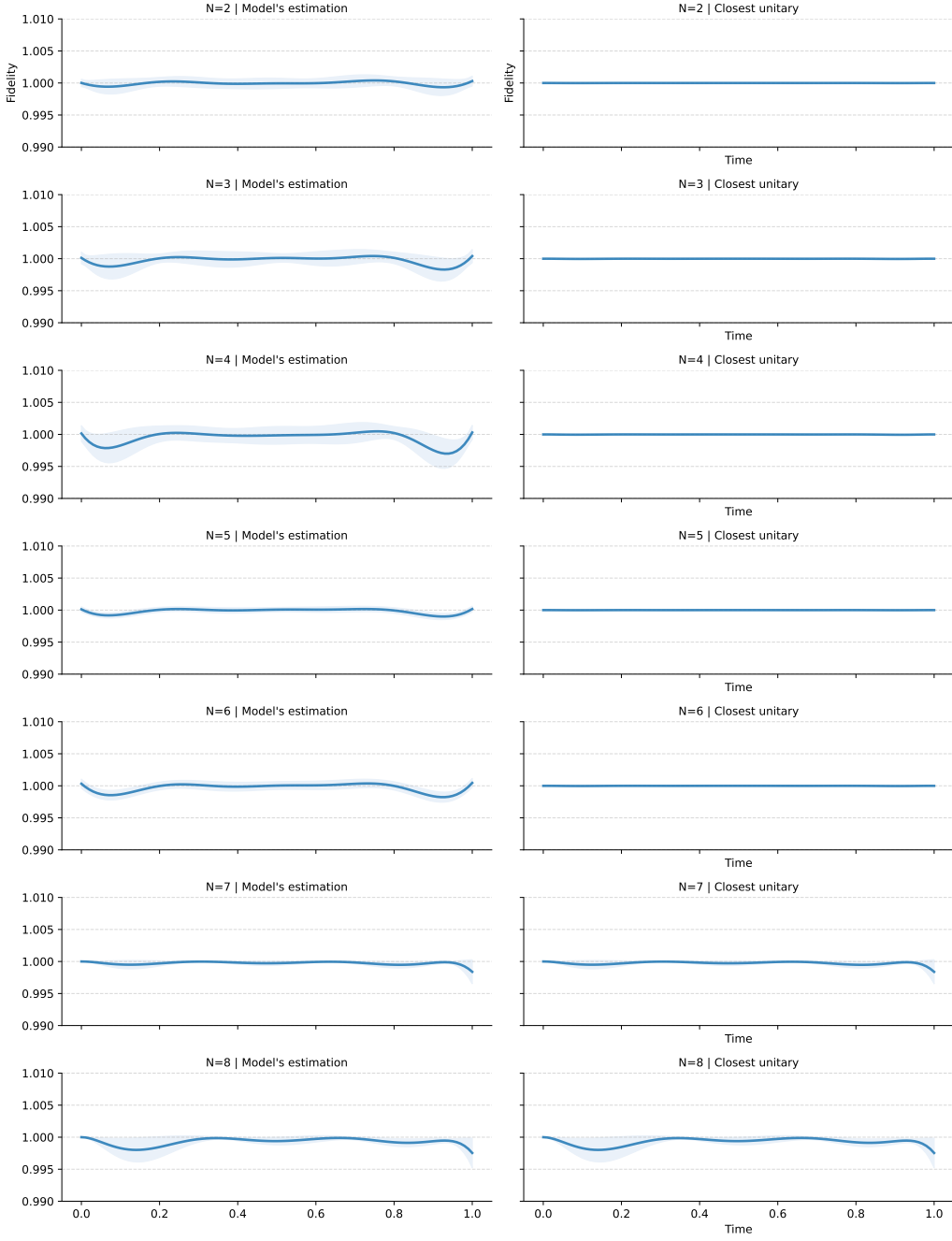


Figure 7: Mean fidelity and standard deviation across N independent training runs for models up to 7 qubits ($N = 100$ for systems up to 6-qubits, $N = 50$ for 7- and 8-qubit systems). The left column reports the fidelity obtained by directly comparing the model-generated matrix with the target unitary, while the right column shows the fidelity between the SVD-corrected closest unitary and the corresponding target unitary.

cost-effective than performing full state tomography at every instant of the evolution. Three datasets were considered, corresponding to time-step sizes of $\Delta t = 0.1, 0.25, 0.5$, and 1.0 . As expected, the model trained with the smallest time step achieved the highest average fidelity, accurately interpolating the unitary time-evolution operators with negligible loss of accuracy.

Remarkably, the model trained with $\Delta t = 1.0$ achieved fidelities comparable to those obtained for $\Delta t = 0.1$. This result suggests that, for the systems studied here, performing QPT at a single time point may already be sufficient to accurately reproduce the system dynamics. Even when trained on data with large temporal gaps, the model maintains high performance at the trained time points, demonstrating strong temporal interpolation capabilities. We expect that the optimal choice of Δt depends on the time dependence of the Hamiltonian: systems exhibiting strong nonlinearities or high-frequency components may require smaller time steps to achieve comparable fidelities. It is well known that generalization of neural-network-based models over extended temporal domains remains a challenging problem in mathematical physics [28, 29]. Consequently, some degradation in performance over larger time intervals is expected; however, this limitation can be mitigated by increasing the number of QPT samples and refining the time discretization.

In addition, a statistical analysis based on multiple independent runs with different Hamiltonians was performed to assess the robustness of the proposed approach. The results show that the models consistently achieve mean fidelities close to 0.99 , with very low standard deviations. No specific time regions were identified in which the interpolation systematically fails or exhibits consistently low fidelity, indicating that the model is able to reliably learn the quantum dynamics given sufficient training data.

A related problem was analyzed in Ref. [30], where a mathematical framework for interpolating unitary matrices using analytical techniques was proposed, yielding promising results. Compared to that approach, the method introduced here offers greater flexibility and can be readily extended to scenarios involving larger system sizes, different Hamiltonians, additional physical constraints, or nonlinear parameter dependencies. Moreover, since the analytical method relies on explicit matrix exponentiation—which becomes computationally expensive for large systems—the deep learning-based framework presented in this work provides a potentially more efficient alternative in applications requiring frequent interpolation of unitary evolution operators.

A notable outcome of this study concerns the behavior of the 7- and 8-qubit models, which rely on an effective Hamiltonian as an intermediate representation. When comparing the learned Hamiltonian with the corresponding target Hamiltonian, we observe that they do not coincide. This indicates that, in its current formulation, the method does not perform Hamiltonian reconstruction. This limitation is expected, as the loss function does not include explicit information about the Hamiltonian itself, but only constraints derived from the unitary evolution. Without additional structural or differential constraints, the model has no incentive to converge toward the true generator of the dynamics. Incorporating information related to derivatives of the unitary operator or enforcing equations of motion at the Hamiltonian level could potentially address this limitation, although doing so would depart from the experimentally motivated training scheme adopted in this work. These directions constitute a promising avenue for future research on Hamiltonian learning.

Overall, the results of this study highlight the potential of deep learning approaches for modeling quantum dynamics, particularly in regimes where data are sparse or discretized. Future work may explore alternative network architectures, extend the framework to non-unitary (open quantum) dynamics, and investigate systems with strong time dependence or chaotic behavior to further assess robustness and generalization. Additionally, integrating this methodology with continuous-measurement protocols could further reduce experimental overhead by exploiting the model’s ability to generate reliable predictions at arbitrary time points.

Acknowledgments

The authors gratefully acknowledge the financial support provided by ANID (Agencia Nacional de Investigación y Desarrollo) through the doctoral scholarship No. 2022-21221096, the research project No. 2023-3230427, FONDECYT 1231940, and the ANID Millennium Science Initiative Program under grant No. ICN17_012. This support has been essential to the development and completion of this research.

A Model architecture

Cases with 2 to 6 qubits

The model's internal data processing involves several fully connected layers. Initially, the input layer takes a scalar input, namely the time. This input is then processed by fully connected layers, which gradually increase the dimensionality of the output vector. After each hidden layer, an activation function is applied, with the hyperbolic tangent function being utilized in this case. Subsequent to processing through the layers, the features obtained are reshaped into a form of $(2, 2^N, 2^N)$, where the first axis is utilized to create the real and imaginary parts of the resulting complex-valued matrix. A comprehensive description of each layer in each model is provided in Table 1.

<i>model2</i> (2 qubits)			<i>model3</i> (3 qubits)		
Layer	Input	Output	Layer	Input	Output
Linear 1	1	64	Linear 1	1	256
Tanh	-	-	Tanh	-	-
Linear 2	64	128	Linear 2	256	512
Tanh	-	-	Tanh	-	-
Linear 3	128	32	Linear 3	512	128
Reshape	32	(2, 4, 4)	Reshape	128	(2, 8, 8)

<i>model4</i> (4 qubits)			<i>model5</i> (5 qubits)		
Layer	Input	Output	Layer	Input	Output
Linear 1	1	512	Linear 1	1	512
Tanh	-	-	Tanh	-	-
Linear 2	512	1024	Linear 2	512	2048
Tanh	-	-	Tanh	-	-
Linear 3	1024	2048	Linear 3	2048	2048
Tanh	-	-	Reshape	2048	(2, 32, 32)
Linear 4	2048	512			
Reshape	512	(2, 16, 16)			

<i>model6</i> (6 qubits)		
Layer	Input	Output
Linear 1	1	1024
Tanh	-	-
Linear 2	1024	4096
Tanh	-	-
Linear 3	4096	8192
Reshape	8192	(2, 64, 64)

Table 1: Architectures of *model2* through *model6*, each representing the generator of a $2^n \times 2^n$ complex unitary matrix from a scalar input t .

Cases with 7 and 8 qubits

For the models handling 7 and 8 qubits, the architecture is similar to that of the previous models, but differs significantly in the output layer. Instead of generating a complex-valued matrix, the output layer is designed to produce a set of time-dependent coefficients corresponding to the Pauli basis representation of the Hamiltonian $H(t)$. The description of the architecture for these models is provided in Table 2.

<i>model7</i> (7 qubits)			<i>model8</i> (8 qubits)		
Layer	Input	Output	Layer	Input	Output
Linear 1	1	50	Linear 1	1	50
Tanh	-	-	Tanh	-	-
Linear 2	50	13	Linear 2	50	15

Table 2: Architectures of *model7* and *model8* designed to generate several real-valued elements within the Pauli basis, all derived from a singular scalar input t .

References

- [1] Juan Terven. Deep reinforcement learning: A chronological overview and methods. *AI*, 6(3), 2025.
- [2] Ihsanul Hoque Sarker. Deep learning: A comprehensive overview on techniques, taxonomy, applications and research directions. *SN Computer Science*, 2(420), 2021.
- [3] Ali Merchant, Simon Batzner, Samuel S. Schoenholz, et al. Scaling deep learning for materials discovery. *Nature*, 624(7990):80–85, 2023.
- [4] Dmitrii Kochkov, Janni Yuval, Ian Langmore, et al. Neural general circulation models for weather and climate. *Nature*, 632(8029):1060–1066, 2024.
- [5] Akhilesh Arya, Sourabh Verma, Prasun Chakrabarti, Tulika Chakrabarti, Ahmed Elngar, Ali-Mohammad Kamali, and Mohammad Nami. A systematic review on machine learning and deep learning techniques in the effective diagnosis of alzheimer’s disease. *Brain Informatics*, 10, 07 2023.
- [6] Omid Panahi. Deep learning in diagnostics. *Journal of Medical Discoveries*, 2(1), 2025.
- [7] Dan Guest, Kyle Cranmer, and Daniel Whiteson. Deep learning and its application to lhc physics. *Annual Review of Nuclear and Particle Science*, 68:161–181, 2018.
- [8] Daniel George and E.A. Huerta. Deep learning for real-time gravitational wave detection and parameter estimation: Results with advanced ligo data. *Physics Letters B*, 778:64–70, 2018.
- [9] Giacomo Torlai, Guglielmo Mazzola, Juan Carrasquilla, et al. Neural-network quantum state tomography. *Nature Physics*, 14:447–450, 2018.
- [10] Peter Cha et al. Attention-based quantum tomography. *Machine Learning: Science and Technology*, 3:01LT01, 2022.
- [11] Daniel Uzcategui-Contreras, Antonio Guerra, Sebastian Niklitschek, and Aldo Delgado. Machine learning approach to reconstruct density matrices from quantum marginals. *Machine Learning: Science and Technology*, 6(2):025068, June 2025.
- [12] M. Raissi, P. Perdikaris, and G.E. Karniadakis. Physics-informed neural networks: A deep learning framework for solving forward and inverse problems involving nonlinear partial differential equations. *Journal of Computational Physics*, 378:686–707, 2019.
- [13] Q Ansel, E Dionis, F Arrouas, B Peaudecerf, S Guérin, D Guéry-Odelin, and D Sugny. Introduction to theoretical and experimental aspects of quantum optimal control. *Journal of Physics B: Atomic, Molecular and Optical Physics*, 57(13):133001, jun 2024.
- [14] I. M. Georgescu, S. Ashhab, and Franco Nori. Quantum simulation. *Rev. Mod. Phys.*, 86:153–185, Mar 2014.
- [15] Dominic W. Berry, Andrew M. Childs, Richard Cleve, Robin Kothari, and Rolando D. Somma. Simulating hamiltonian dynamics with a truncated taylor series. *Phys. Rev. Lett.*, 114:090502, Mar 2015.

- [16] Mária Kieferová, Artur Scherer, and Dominic W. Berry. Simulating the dynamics of time-dependent hamiltonians with a truncated dyson series. *Phys. Rev. A*, 99:042314, Apr 2019.
- [17] Michael Schilling, Francesco Preti, Matthias M. Müller, Tommaso Calarco, and Felix Motzoi. Exponentiation of parametric hamiltonians via unitary interpolation. *Phys. Rev. Res.*, 6:043278, Dec 2024.
- [18] Mogens Dalgaard and Felix Motzoi. Fast, high precision dynamics in quantum optimal control theory. *Journal of Physics B: Atomic, Molecular and Optical Physics*, 55(8):085501, apr 2022.
- [19] Ariel Norambuena, Marios Mattheakis, Francisco J. González, and Raúl Coto. Physics-informed neural networks for quantum control. *Physical Review Letters*, 132(1):010801, 2024.
- [20] Liangyu Che, Chao Wei, Yulei Huang, Dafa Zhao, Shunzhong Xue, Xinfang Nie, Jun Li, Dawei Lu, and Tao Xin. Learning quantum hamiltonians from single-qubit measurements. *Phys. Rev. Res.*, 3:023246, Jun 2021.
- [21] Chen-Di Han, Bryan Glaz, Mulugeta Haile, and Ying-Cheng Lai. Tomography of time-dependent quantum hamiltonians with machine learning. *Phys. Rev. A*, 104:062404, Dec 2021.
- [22] Antonio Guerra. Pinn unitary estimation, 2025.
- [23] T. Oka and H. Aoki. Photovoltaic hall effect in graphene. *Physical Review B*, 79:081406, 2009.
- [24] André Eckardt. Colloquium: Atomic quantum gases in periodically driven optical lattices. *Reviews of Modern Physics*, 89:011004, 2017.
- [25] George Em Karniadakis, Ioannis G. Kevrekidis, Lu Lu, Paris Perdikaris, Sifan Wang, and Liu Yang. Physics-informed machine learning. *Nature Reviews Physics*, 3:422–440, 2021.
- [26] Tangyou Huang, Akshay Gaikwad, Ilya Moskalenko, Anuj Aggarwal, Tahereh Abad, Marko Kuzmanovic, Yu-Han Chang, Ognjen Staničević, Emil Hogedal, Christopher Warren, Irshad Ahmad, Janka Biznárová, Amr Osman, Mamta Dahiya, Marcus Rommel, Anita Fadavi Rousari, Andreas Nylander, Liangyu Chen, Jonas Bylander, Gheorghe Sorin Paraoanu, Anton Frisk Kockum, and Giovanna Tancredi. Quantum process tomography with digital twins of error matrices, 2025.
- [27] Renan Cabrera, Ofer M Shir, Rebing Wu, and Herschel Rabitz. Fidelity between unitary operators and the generation of robust gates against off-resonance perturbations. *Journal of Physics A: Mathematical and Theoretical*, 44(9):095302, feb 2011.
- [28] Hang Zhou, Han Wu, Brian Sheil, and Zhuhong Wang. A self-adaptive physics-informed neural networks method for large strain consolidation analysis. *Computers and Geotechnics*, 181:107131, 2025.
- [29] Z. Li. A review of physics-informed neural networks. *Applied and Computational Engineering*, 133:164–172, 2025.
- [30] Michael Schilling, Francesco Preti, Matthias M. Müller, Tommaso Calarco, and Felix Motzoi. Exponentiation of parametric hamiltonians via unitary interpolation. *Phys. Rev. Res.*, 6:043278, Dec 2024.